

# New Method for Jet Noise Reduction in Turbofan Engines

Dimitri Papamoschou\*

University of California, Irvine, Irvine, California 92697-3975

**A new method for reducing large-scale mixing noise from dual-stream jets is presented. The principle is reduction of the convective Mach number of turbulent eddies that produce intense downward sound radiation. In a jet representing the coaxial exhaust of a turbofan engine, this is achieved by tilting downward, by a few degrees, the bypass (secondary) plume relative to the core (primary) plume. The misalignment of the two flows creates a thick low-speed secondary core on the underside of the high-speed primary flow. The secondary core reduces the convective Mach number of primary eddies, thus hindering their ability to generate sound that travels to the downward acoustic far field. Tilting of the bypass stream is possible by means of fixed or variable vanes installed near the exit of the bypass duct. Subscale aeroacoustic experiments simulated the exhaust flow of a turbofan engine with bypass ratio 6.0. Deflection of the bypass stream resulted in suppression of the peak overall sound pressure level by 4.5 dB and the effective perceived noise level by 2.8 dB. For the nozzle configuration used, the thrust loss is estimated at around 0.5% with the vanes activated and 0.15% with the vanes deactivated.**

## Nomenclature

$A$	= duct cross-sectional area
$a$	= mean speed of sound
$a_{2D}$	= two-dimensional lift curve slope
$B$	= bypass ratio, $\dot{m}_s/\dot{m}_p$
$C_D$	= total drag coefficient of vane
$C_{D,p}$	= parasite drag coefficient of vane
$C_L$	= lift coefficient of vanes
$c$	= chord length of vane airfoil
$D$	= nozzle diameter or total drag of vanes
$D_i$	= inviscid induced drag of vanes
$f$	= frequency
$K$	= induced viscous drag factor
$L$	= lift of vanes
$M$	= Mach number
$M_c$	= convective Mach number
$\dot{m}$	= mass flow rate
$N_v$	= number of vanes
$p$	= static pressure
$r$	= distance from jet exit
$S_v$	= vane planform area
$T$	= thrust
$U$	= nozzle-exit or internal velocity
$U_c$	= convective velocity
$u$	= mean axial velocity of jet plume
$x$	= axial distance from jet exit
$y$	= radial distance from jet centerline
$\alpha$	= vane angle of attack
$\beta$	= vane impact coefficient; Eq. (12)
$\epsilon$	= deflection angle of bypass stream
$\theta$	= polar angle relative to jet axis
$\rho$	= density
$\phi$	= azimuth angle relative to downward vertical

$v$	= condition at axial location of vanes
$\infty$	= ambient (flight) conditions

## I. Introduction

**A**IRCRAFT noise is an issue of enormous environmental, financial, and technological impact. There are two main sources of noise in today's commercial aircraft engines: fan/compressor noise and jet noise. Jet noise comprises turbulent mixing noise and, in the case of imperfectly expanded jets, shock noise.<sup>1</sup> Turbulent mixing noise is very difficult to control, and so its suppression remains a challenge. It is generally agreed that turbulent shear-flow mixing causes two types of noise: sound produced by the large-scale eddies and sound generated by the fine-scale turbulence.<sup>2</sup> The former is very intense and directional and propagates at an angle close to the jet axis. The latter is mostly uniform and affects the lateral and upstream directions.

The increase in bypass ratio over the last three decades has resulted in a dramatic suppression in the jet noise of turbofan engines. Modern engines are so quiet that further reduction in noise becomes extremely challenging. The success of the high-bypass engine is offset, to some degree, by the increasing volume of aircraft operations. This creates more environmental and political pressures for quieter aircraft. Today the most successful technique for reducing jet noise from high-bypass engines involves the installation of chevron mixers on the exhaust nozzles.<sup>3</sup> However, the ever increasing need for quieter engines requires exploration of alternative techniques that could be used by themselves or in conjunction with existing methods. The technique described in this paper targets noise from large-scale eddies.

Large-scale mixing noise has been modeled by treating turbulent eddies as instability waves. At the simplest level, one can approximate the turbulent interface between the jet and the ambient as a wavy wall propagating with a convective speed  $U_c$ . When  $U_c$  is supersonic, Mach waves are radiated from the wall. When  $U_c$  is subsonic, disturbances decay exponentially away from the wall. The notion of sound radiation from large-scale flow instabilities was first confirmed in the supersonic jet experiments of McLaughlin et al.<sup>4</sup> and the subsequent experiments of Troutt and McLaughlin.<sup>5</sup> In those experiments, the orientation, wavelength, and frequency of the measured acoustic radiation were found to be consistent with the Mach wave concept. The linear stability analysis of Tam and Burton<sup>6</sup> further solidified this idea by showing that the sound emitted by a supersonic wave matched the trends found in the aforementioned experiments. Since then, a large volume of experimental and theoretical works have addressed various aspects of this problem. For example, see Refs. 7–9.

## Subscripts

$p$	= primary (core) exhaust
$s$	= secondary (bypass) exhaust

Received 26 August 2003; revision received 4 May 2004; accepted for publication 28 May 2004. Copyright © 2004 by Dimitri Papamoschou. Published by the American Institute of Aeronautics and Astronautics, Inc., with permission. Copies of this paper may be made for personal or internal use, on condition that the copier pay the \$10.00 per-copy fee to the Copyright Clearance Center, Inc., 222 Rosewood Drive, Danvers, MA 01923; include the code 0001-1452/04 \$10.00 in correspondence with the CCC.

\*Professor, Department of Mechanical and Aerospace Engineering, Associate Fellow AIAA.

Mach wave emission is governed by the convective Mach number  $M_c$  of the instability wave. When  $M_c$  is supersonic, strong Mach wave radiation can be easily captured in instantaneous photographs of jets. For subsonic  $M_c$ , the growth–decay nature of instability waves creates a spectrum of phase speeds, part of which is supersonic.<sup>2</sup> The resulting Mach wave emission is not as intense or nonlinear as its supersonic counterpart but still constitutes the strongest source of sound. As  $M_c$  becomes more subsonic, Mach wave emission weakens rapidly. Reduction of  $M_c$ , thus, has the potential of being an effective method for noise suppression. Recent works have demonstrated noise suppression from supersonic jets by application of a parallel secondary flow around the primary jet. The secondary flow reduces the convective Mach number of the primary eddies and, hence, curtails their ability to generate sound that radiates to the far field. Eccentric nozzles were very effective in this respect because the thick part of the secondary flow covered most of the noise sources on the underside of the jet and, hence, suppressed downward-emitted sound.<sup>10,11</sup>

It became apparent, however, that offsetting the nozzles to an eccentric geometry did not offer an attractive engineering solution for high-bypass engines. Notwithstanding the possible losses and imbalances caused by the new flowpath, an eccentric arrangement would require a new nacelle structure and radical redesign of propulsion systems such as thrust reversers. An alternative was sought that would provide equal or greater acoustic benefit while minimizing redesign of the propulsion system. This paper discusses such an alternative method and provides some background on the fundamental fluid mechanics behind it. It also extends prior noise suppression efforts of the same general approach, which dealt with supersonic jets,<sup>11,12</sup> to lower-speed jets associated with subsonic commercial engines.

## II. Noise Reduction Approach

### A. Convective Mach Number $M_c$

The large-scale structures in the shear layers of a turbulent jet can be modeled as instability waves traveling with a convective speed  $U_c$ . When  $\eta(x, t)$  describes the vortex sheet between the jet and a quiescent ambient, a simple traveling wave is given by

$$\eta(x, t) = Ae^{i(x-U_c t)} \quad (1)$$

where a wave number of unity has been chosen for simplicity. The convective Mach number of the instability wave is

$$M_c = U_c/a_\infty \quad (2)$$

With the amplitude  $A$  constant, the instability radiates sound to the far field when  $M_c > 1$ . The next level of realism is to consider the nonparallel (growing) nature of the mean flow. In this case, linear stability theory shows that a perturbation at fixed frequency amplifies and then decays with axial distance. The vortex sheet now assumes the form of a wave packet:

$$\eta(x, t) = A(x)e^{i(x-U_c t)} \quad (3)$$

Tam and Burton<sup>6</sup> showed that the amplitude modulation  $A(x)$  creates a continuous spectrum of phase speeds. For finite  $M_c$ , part of this spectrum is supersonic. Thus, even a subsonically traveling wave can generate Mach waves. This consequence of the growth–decay envelope was further investigated by Crighton and Huerre,<sup>13</sup> Tam and Chen,<sup>1</sup> and Avital et al.<sup>14</sup> More recently, direct numerical simulation of a Mach 0.9 jet<sup>15</sup> revealed that the radiating component of the noise source, at single frequency, is a modulated wave of the type captured by Eq. (3) and shown in Fig. 1.

The creation of a continuous spectrum of phase speeds by the amplitude modulation  $A(x)$  becomes evident when we write  $\eta(x, t)$  in Fourier space:

$$\eta(x, t) = \frac{1}{2\pi} \int_{-\infty}^{\infty} \hat{A}(k-1) \exp \left[ ik \left( x - \frac{U_c}{k} t \right) \right] dk \quad (4)$$

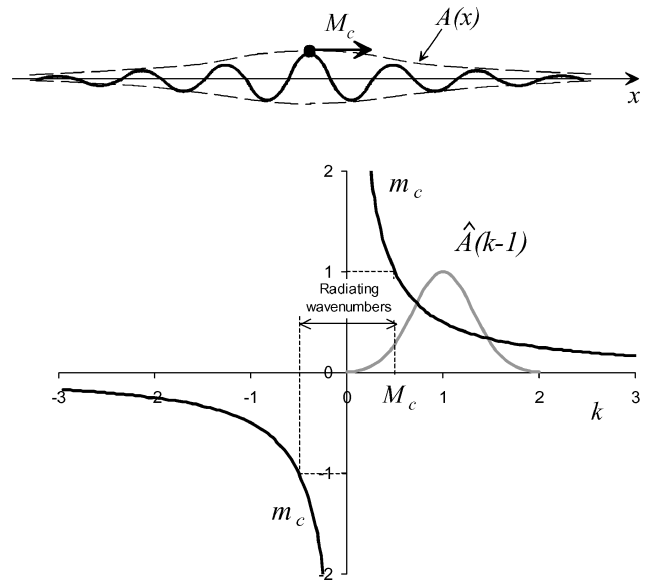


Fig. 1 Phase Mach number vs wave number for  $M_c = 0.5$ .

Equation (4) shows that the wave packet is a superposition of individual simple waves, each with wave number  $k$ , amplitude  $\hat{A}(k-1) dk/(2\pi)$ , and phase speed  $U_c/k$ . The phase Mach number of each individual wave is

$$m_c = (U_c/k)/a_\infty = M_c/k \quad (5)$$

Instabilities with  $|k| < M_c$  are supersonic and radiate to the far field; those with  $|k| > M_c$  are subsonic and decay rapidly with distance away from the jet axis. Figure 1 plots  $m_c$  vs  $k$  for  $M_c = 0.5$ . Also shown is a generic  $\hat{A}(k-1)$ . The energy contained in the radiating sound field is governed by the integral of  $\hat{A}(k-1)$  from  $-M_c$  to  $M_c$ .

Clearly, reducing  $M_c$  will reduce the amount of energy radiated to the far field. Meaningful reduction of  $M_c$  must take into account the thermodynamic cycle of the engine, that is, the exhaust conditions (velocity and Mach number) should be considered fixed. Under this constraint, reduction of  $M_c$  entails controlling  $U_c$  or controlling the medium surrounding the instability wave. Control of  $U_c$  would involve some type of forcing that reduces  $U_c$  throughout the noise source region of the jet. This region comprises the potential core and a certain distance past the end of the potential core. There is no experimental evidence that such control is feasible. Controlling the medium surrounding the jet is more plausible because it involves manipulation of a secondary stream flowing adjacent to the primary stream.

Source location experiments indicate that most of the large-scale turbulent mixing noise comes from the region near the end of the potential core.<sup>16–19</sup> Any scheme to reduce noise via reduction of the convective Mach number must take this fact into account. In other words, it is not sufficient to reduce  $M_c$  near the nozzle exit. It should be reduced throughout the high-speed region of the jet. The length of this region is on the order of 10–20 jet diameters.

### B. Reduction of $M_c$

Today practically all engines powering commercial and military aircraft are of the turbofan type. The existence of a secondary flow, the bypass stream, provides an opportunity for reduction of  $M_c$  to suppress noise from large-scale turbulent structures. This section overviews the effect of the mean flowfield on the distribution of  $M_c$  in dual-stream jets.

The initial region of a dual-stream jet consists of two shear layers: the primary shear layer between the primary and secondary streams and the secondary shear layer between the secondary and ambient streams (Fig. 2). The primary shear layer encloses the primary potential core. The region between the primary and secondary shear layers defines the secondary core, which contains an initial potential

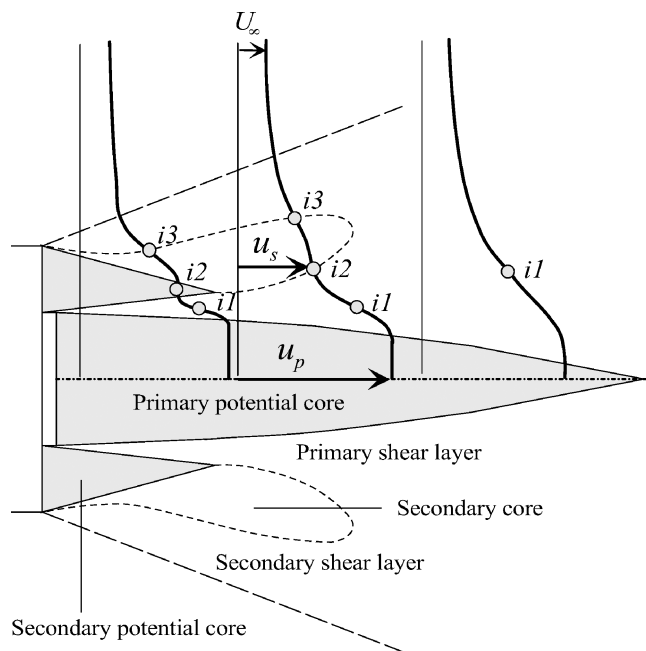


Fig. 2 Basic elements of mean flow in a dual-stream jet.

region followed by a nonpotential region. This broad definition of the secondary core is essential for understanding the acoustic benefit of certain dual-stream configurations. In many practical cases, for instance, in coaxial jets of turbofan engines, the secondary core ends upstream of the end of the primary core. The flow past the end of the secondary core consists of a single shear layer between the jet centerline and the ambient stream, thus having the characteristics of a single-stream jet. It is useful, therefore, to divide the jet flow into two regions: the compound region, that is, the region before the end of the secondary core, and the simple region, which is the region past the end of the secondary core. The extent of the compound region, relative to the length of the primary potential core, is critical for noise reduction.

The relations for the primary and secondary convective Mach numbers are as follows:

$$M_{c_p}(x) = \frac{U_{c_p}(x) - u_s(x)}{a_s(x)} \quad (6)$$

$$M_{c_s}(x) = \frac{U_{c_s}(x) - U_\infty}{a_\infty} \quad (7)$$

Application of Eqs. (6) and (7) requires knowledge of the velocity distributions  $u_p(x)$  and  $u_s(x)$  that define the two shear layers. Once these distributions are known, the convective velocities  $U_{c_p}(x)$  and  $U_{c_s}(x)$  can be estimated from empirical models based on direct measurements of  $U_c$  in jets and shear layers.<sup>20</sup>

The fast velocity of the primary shear layer,  $u_p(x)$ , is the maximum mean velocity of the jet. Experiments show that it occurs on the axis of the primary jet, even for configurations with asymmetric secondary flow. Definition of the slow velocity of the primary shear layer (fast velocity of the secondary shear layer),  $u_s(x)$ , is not as straightforward. It is clear that  $u_s(x) = U_s$  inside the potential region of the secondary core. Downstream of the potential region, however, definition of  $u_s(x)$  becomes problematic. Experimental velocity profiles show a distinct secondary layer for a finite distance past the end of the secondary potential core. This is particularly noticeable in jets from eccentric nozzles. (For example, see Fig. 4c of Ref. 21.) It would be unreasonable, therefore, to assume that the effect of the secondary flow ceases immediately past the end of the secondary potential core.

The resolution of dilemma entails a consistent, unambiguous way to detect the presence of a secondary shear layer. This is done here by examining the inflection points of the radial velocity profile.

The compound region of the jet is characterized by three inflection points:  $i1$ ,  $i2$ , and  $i3$ , marked in Fig. 2. The second inflection point,  $i2$ , defines the outer edge of the primary shear layer (inner edge of the secondary shear layer). Dahl and Morris,<sup>22</sup> in their mean flow model for coaxial jets, used basically the same criterion to distinguish the two shear layers. Thus,  $u_s(x) = u[x, y_{i2}(x)]$ . The three inflection points persist for a certain distance past the end of the secondary potential core. At some point, two of them disappear, and the profile reduces to that of a single-stream jet. The downstream distance where the number of inflection points reduces from three to one marks the end of the secondary core. Beyond this point,  $u_s = U_\infty$  and  $a_s = a_\infty$  in Eq. (6). Also,  $M_{c_s}$  [Eq. (7)] ceases to exist.

To reduce  $M_{c_p}$  throughout the jet, it is necessary to have a long secondary core that covers the entire primary potential core. Eccentric nozzle arrangements have proven very effective in this respect. The experiments of Murakami and Papamoschou<sup>21</sup> showed that eccentric nozzles shorten the length of the primary potential core and double the length of the secondary potential core on the underside of the jet. The downward noise emission of the eccentric jet was much lower than the noise emission of the equivalent coaxial jet.<sup>10</sup> A critical flow feature that was not emphasized in Ref. 21 is the remarkable persistence of the inflection point  $i2$  in the eccentric cases with velocity ratio  $U_s/U_p = 0.67$ . Reexamination of the relevant data of Ref. 21 shows that the inflection point  $i2$  (and, of course, the inflection points  $i1$  and  $i3$ ) can be identified all of the way to the end of the measurement region. In other words, when the nozzles were off setting, the secondary core on the underside of the jet became longer than the primary potential core. This may explain the acoustic benefit of eccentric configurations even with small diameter ratio and small secondary mass flow rate.<sup>10</sup>

This paper focuses on a different approach of obtaining a long secondary core: tilting the secondary stream downward relative to the axis of the primary stream while maintaining a coaxial nozzle exit. This is thought to be more practical than an eccentric configuration and offers the possibility of on-demand control of noise. A comprehensive study of the mean flow of dual-stream jets<sup>23</sup> shows that tilting of the secondary flow produces an effect similar to that obtained by offsetting the nozzles. Selected results from this study are presented here to provide insight into the overall approach of convective Mach number reduction. The jets were composed of air at ambient total temperature. Flow conditions were  $M_p = 1.0$ ,  $M_s = 0.65$ , and  $B = 1.0$ . The velocity ratio was  $U_s/U_p = 0.7$ , which matches the velocity ratio of commercial turbofan engines at takeoff power. The mean axial velocity of the jet plume  $u$  was computed from pitot pressure surveys.

Figure 3 plots isocontours of  $u/U_p$  for jets issuing from the following nozzles: clean coaxial, eccentric, and coaxial with vanes in the secondary stream. The vanes imparted a downward tilt to the secondary plume. Focusing in the region near the end of the potential core, defined here by the contour  $u/U_p = 0.9$ , we make the following observations. For the clean coaxial jet, there is no indication of a secondary core; the secondary stream becomes fully mixed with the primary flow well upstream of the end of the primary potential core. In the eccentric and deflection cases, however, there is a distinct core of low-speed flow on the underside of the jet. To quantify these findings, Fig. 4 plots the distributions of  $u_p(x)$  and  $u_s(x)$  obtained by the methods outlined earlier and shown in Fig. 2. For the coaxial case,  $u_s(x)$  decays very rapidly past the end of the secondary core. In the eccentric and deflected jets, the decay of  $u_s(x)$  is much more gradual and reflects the long secondary cores created in those jets. The decay rate in the deflected jet is a little faster than that in the eccentric case.

With use of the convective Mach number model of Murakami and Papamoschou,<sup>20</sup> the distributions  $M_{c_p}(x)$  and  $M_{c_s}(x)$  are computed and plotted in Fig. 5. Note that, because the experiments used air at room temperature, the convective Mach numbers calculated here are much lower than those in hot jets. However, the trends to be presented are expected to be the same for hot jets with similar velocity ratio as cold jets. For the coaxial jet,  $M_{c_p}$  is very low subsonic at the jet exit but rises rapidly past the end of the secondary core and reaches the peak value of 0.58 at the axial location where the

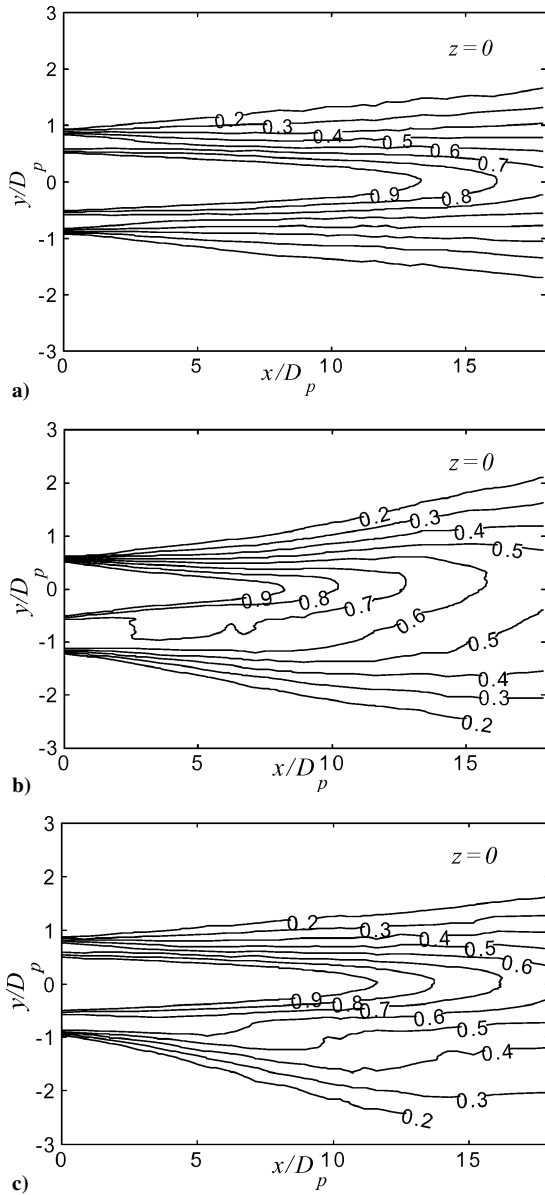


**Fig. 3** Isocontours of mean velocity, normalized by the primary exit velocity, on the vertical centerplane of the following jets: a) clean coaxial, b) eccentric, and c) coaxial with downward deflection of the secondary stream.

secondary core ends ( $x/D_p = 4$ ). Offsetting the nozzles to an eccentric arrangement reduces the maximum value of  $M_{c_p}$  on the underside of the jet to 0.15. The very slow decay of  $u_s(x)$  creates a long distribution of  $M_{c_s}$ , starting from 0.32 at the nozzle exit and ending at 0.25 near the end of the measurement region. This suggests that the secondary layer now becomes the dominant noise source. In the deflected jet, the maximum value of  $M_{c_p}$  is 0.25, higher than in the eccentric case, but the distribution of  $M_{c_s}$  is shorter and its average value is lower. The deflected jet seems to achieve a better balance between the distributions of  $M_{c_p}$  and  $M_{c_s}$  than does the eccentric jet. Of course this depends on the tilt angle and other details of the deflection mechanism. Nevertheless, the deflection approach allows more degrees of freedom to manipulate the distributions of  $M_{c_p}$  and  $M_{c_s}$  (not only in the downward direction but also in the sideline direction) for optimal noise reduction. The next section gives more details on the aerodynamics of the tilting of the bypass stream.

### C. Deflection of the Bypass Stream

The rationale for tilting the bypass plume relative to the core plume is to thicken the bypass stream in the vicinity of the strongest

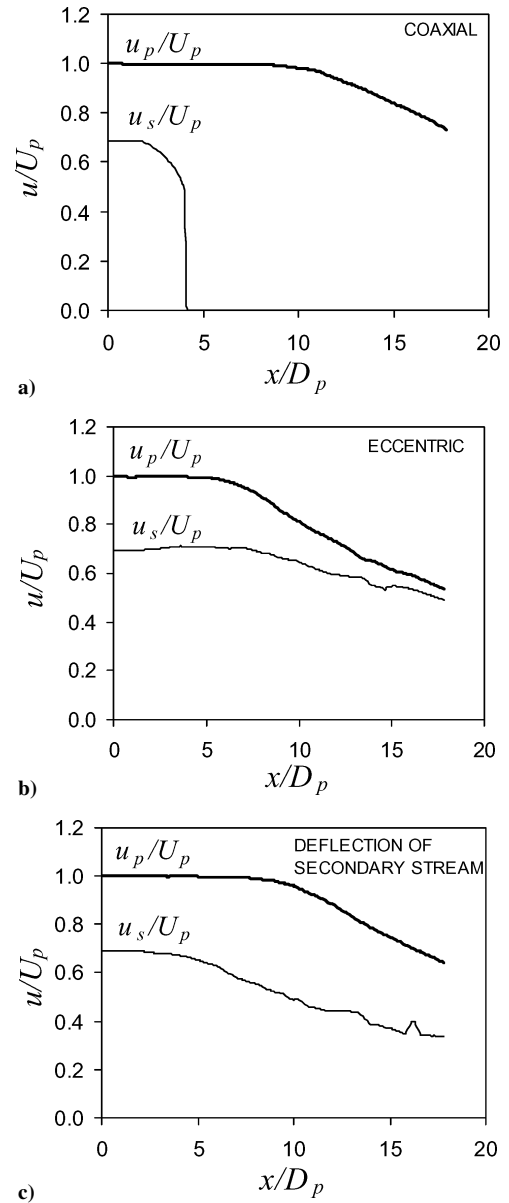


**Fig. 4** Distribution of velocities defining the primary and secondary shear layers for the jets of Fig. 3: a) clean coaxial jet, b) underside of eccentric jet, and c) underside of coaxial jet with deflection of the bypass stream.

sources of noise (largest eddies) of the core stream. The principle of deflection of the bypass stream is shown in Fig. 6. As mentioned earlier, the strongest sources of noise reside near the end of the primary potential core. Given that the length of the primary potential core is on the order of 15 primary exit diameters (for example, see Fig. 3), one can make an order-of-magnitude estimate that the desired tilt angle is a modest 1/15 or 4 deg. The tilt entails a transverse (lift) force  $L$  applied to the bypass stream near its exit. Here we consider generation of this force by vanes immersed in the bypass stream.

The vanes could be placed inside or outside the bypass duct. Placement inside the duct has the advantage of a subsonic environment and, thus, avoidance of serious shock losses. There is a limit as to how deep inside the duct one should place the vanes: The aerodynamic force of the vanes should be transmitted to the momentum flux exiting the duct and not to the duct walls. Otherwise the effect of vane lift will be lessened or canceled by transverse forces acting on the duct walls. When it is assumed that the lift of the vanes is transmitted entirely to the exhaust plume, and that all of the flow angles are small, the integral momentum equation gives the following

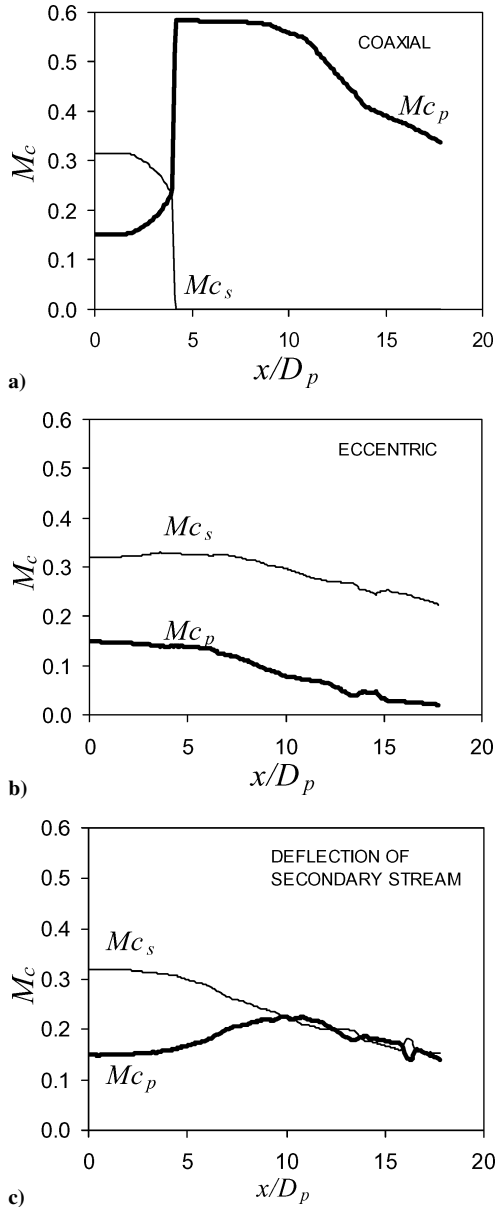


**Fig. 5** Distribution of convective Mach numbers corresponding to the velocity distributions of Fig. 4: a) clean coaxial jet, b) underside of eccentric jet, and c) underside of coaxial jet with deflection of the bypass stream.

relation between the tilt angle of the bypass stream and the lift force of the vanes:

$$\epsilon = L / \dot{m}_s U_s \tag{8}$$

The ideal thrust loss of the bypass stream is connected to the cosine of the tilt angle. We can draw an analogy between the ideal thrust loss of the jet and the inviscid induced (lift-dependent) drag of a finite wing. In both instances, the momentum flux is deflected downward to generate lift; the tilting of the momentum vector results in induced drag. (For a treatment of the finite wing as a flow deflector, see Ref. 24.) The ideal thrust loss of the jet is, thus, equal to the inviscid induced drag of the vanes,  $D_i$ , given by the relation

$$D_i = \dot{m}_s U_s (1 - \cos \epsilon) \approx \dot{m}_s U_s (\epsilon^2 / 2)$$

where the small angle approximation  $\cos \epsilon \approx 1 - \frac{1}{2} \epsilon^2$  was used. When combined with Eq. (8),

$$D_i = L (\epsilon / 2) \tag{9}$$

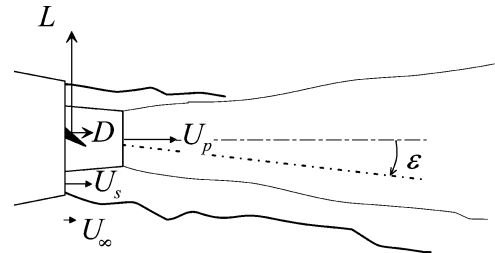


**Fig. 6** Principle of deflection of the bypass stream.

In the following analysis, we consider the aerodynamics of vanes installed inside the bypass duct. There are no published works on this type of flow, and so the intent of the analysis is to generate some fundamental insight into the basic aerodynamics. We will attempt some predictions of lift and drag with the understanding that these will be preliminary estimates to be validated in future computations and experiments. Each vane is assumed to be a constant-chord airfoil that spans the entire width of the annulus of the bypass duct. Because the airfoil is bounded by sidewalls, it would appear that, save for viscous end-wall effects, it behaves as an infinite two-dimensional airfoil. If this were true, and wave drag were excluded, there would be no inviscid-induced drag. We know, however, that there is a thrust loss, given by Eq. (9), even in the limit of inviscid, shock-free flow. The integral view of the jet, captured by Eqs. (8) and (9), and the detailed view of the vane airfoils can be reconciled by considering  $\epsilon/2$  in Eq. (9) as the downwash angle in the vicinity of the vane. The total drag of the vane consists of the parasite drag, the viscous-induced drag, and the inviscid-induced drag given by Eq. (9). With the parasite drag coefficient  $C_{Dp}$ , the viscous-induced drag is assumed to scale as  $K C_{Dp} C_L^2$  (Ref. 24). Thus,

$$C_D = C_{Dp} + C_{Dp} K C_L^2 + C_L (\epsilon / 2) \tag{10}$$

When it is assumed that all of the vanes have identical characteristics and are mounted at azimuth angles close to  $\phi = 90$  deg, the total lift of the vanes is

$$L = N_v C_L \frac{1}{2} \rho_v U_v^2 S_v$$

When divided by  $\dot{m}_s U_s$ ,  $\dot{m}_s = \rho_s U_s A_s = \rho_v U_v A_v$  is noted, and inserting Eq. (9),

$$\epsilon / 2 = \beta C_L \tag{11}$$

where  $\beta$  is defined here as the vane impact coefficient,

$$\beta = \frac{1}{4} (N_v S_v / A_v) (U_v / U_s) \tag{12}$$

When Eq. (11) is used, the drag coefficient [Eq. (10)] can be expressed in terms of the vane impact coefficient:

$$C_D = C_{Dp} + (K C_{Dp} + \beta) C_L^2 \tag{13}$$

The lift coefficient vs angle-of-attack relation is

$$C_L = a_{2D} (\alpha - \epsilon / 2)$$

When Eq. (11) is inserted,

$$C_L = \frac{a_{2D}}{1 + a_{2D} \beta} \alpha \tag{14}$$

$$\epsilon = \frac{2 \beta a_{2D}}{1 + a_{2D} \beta} \alpha \tag{15}$$

To obtain the vane drag-to-lift ratio as a function of the deflection angle, Eq. (13) is divided by  $C_L$  and is combined with Eq. (11) to give

$$C_D / C_L = 2 C_{Dp} \beta / \epsilon + (\epsilon / 2) (K C_{Dp} / \beta + 1) \tag{16}$$

The total drag of the vanes is  $D = LC_D/C_L$ . When Eqs. (8) and (16) are applied,

$$D = \dot{m}_s U_s \left[ 2C_{D_p} \beta + (\epsilon^2/2) \left( KC_{D_p} / \beta + 1 \right) \right] \quad (17)$$

To obtain the total drag of the vanes as a fraction of the total thrust, Eq. (18) is divided by  $T_{\text{total}} = \dot{m}_p(U_p - U_\infty) + \dot{m}_s(U_s - U_\infty)$ :

$$\frac{D}{T_{\text{total}}} = \left[ 2C_{D_p} \beta + \frac{\epsilon^2}{2} \left( \frac{KC_{D_p}}{\beta} + 1 \right) \right] \frac{BU_s}{U_p - U_\infty + B(U_s - U_\infty)} \quad (18)$$

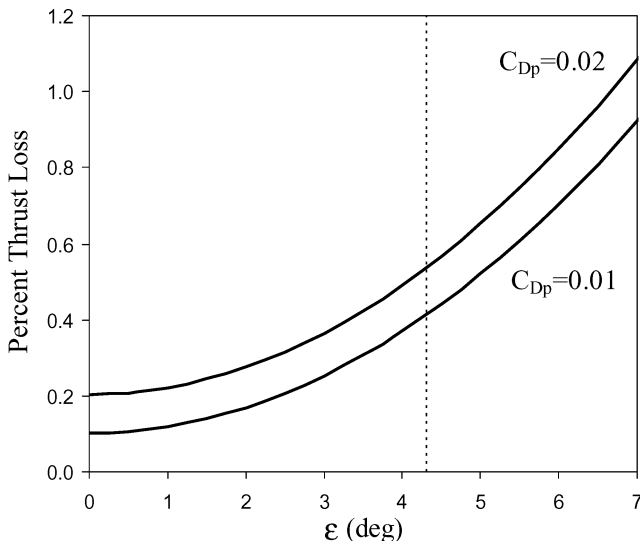
Equation (18) gives the thrust loss. It is valid for perfectly expanded flow and under the assumptions used in its derivation. Extension to imperfectly expanded flow is straightforward but beyond the scope of this paper. Clearly, the efficiency of this noise suppression scheme depends on the parasite drag coefficient  $C_{D_p}$  of the vane airfoils and the vane impact coefficient  $\beta$ . Both should be minimized. Minimization of  $\beta = \epsilon/2C_L$  is constrained by the maximum lift coefficient before stall. To avoid flow separation on the vanes, it would be prudent to use  $C_{L_{\text{max}}} \sim 1$ . For a deflection angle  $\epsilon = 4$  deg, for example, the vane impact coefficient should not be less than 0.035. However, if the vanes were placed in a favorable pressure gradient, that is, inside the convergent section of the bypass duct, larger values of  $C_{L_{\text{max}}}$  may be possible without flow separation. To minimize  $C_{D_p}$ , it is important to use thin, supercritical airfoils with good lift-to-drag ratios up to transonic Mach numbers. The problem of vanes placed inside the bypass duct lends itself to the shape optimization techniques recently developed for transonic airfoils.<sup>25</sup> The additional element of an externally imposed favorable pressure gradient, which can delay shock losses and separation, creates the potential for efficiencies higher than those possible in a zero-pressure-gradient environment.

Figure 7 plots the predictions of Eq. (18) for the takeoff conditions listed in Table 1 and  $U_\infty = 80$  m/s. The following coefficients are used:  $\beta = 0.05$  (a value corresponding to the experiments described later),  $K = 0.4$ , and  $C_{D_p} = 0.01$  and  $0.02$ . The lower value of  $C_{D_p}$

**Table 1** Exit flow conditions

Quantity	Primary	Secondary
Diameter, mm	10.0 <sup>a</sup>	25.4
Velocity, m/s	460	335
Mach number	0.86	0.95
Bypass ratio	—	6.0

<sup>a</sup>Effective (area-based) diameter.



**Fig. 7** Estimated percent thrust loss vs deflection angle of bypass stream for flow of this study: ---, estimate of the deflection angle in present experiment.

represents an efficient, supercritical airfoil at high-subsonic Mach number.<sup>25</sup> The higher value represents a standard thin airfoil at near-sonic Mach number.<sup>26</sup> With  $C_{D_p} = 0.015$ , the average of the two limits, the thrust loss is 0.5% at  $\epsilon = 4.3$  deg and 0.15% at  $\epsilon = 0$  deg. Prediction of losses at cruise requires generalization of the preceding relations to imperfectly expanded flows and use of engine cycle analysis to determine the exit velocities and Mach numbers. Details will be presented in future publications, but preliminary estimates indicate that the losses are similar to those computed for takeoff.

### III. Experimental Setup

The intent of the experiments was to test the new noise reduction approach on jets that approximate the exhaust conditions of commercial turbofan engines with bypass ratio 6. Noise testing was conducted in the University of California, Irvine (UCI), Jet Aeroacoustics Facility, shown schematically in Fig. 8 and described in earlier publications.<sup>10</sup> Dual-stream jets with exit conditions listed in Table 1 were generated. The jets were composed of helium–air mixtures, which duplicate accurately the fluid mechanics and acoustics of hot jets.<sup>27</sup> Velocities and Mach numbers were kept to within 0.5% of their target values.

Noise measurements were conducted inside an anechoic chamber using a 2.3-mm condenser microphone (Brüel and Kjør 4138) with frequency response of 140 kHz. The microphone was mounted on a pivot arm and traced a circular arc centered at the jet exit with radius  $r = 94D_{p,\text{eff}}$ . Earlier experiments determined that this distance is well inside the acoustic far field.<sup>28</sup> Figure 8 shows the overall setup and the range of polar angles covered. The sound spectra were corrected for the microphone frequency response, free-field response, and atmospheric absorption. All of the acoustic data presented here, with exception of the perceived noise level, are referenced to  $r/D_{p,\text{eff}} = 100$ . Repetition of an experiment under varying temperature and relative-humidity conditions (typically from 20 to 50%) yields spectra that differ by, at most, 0.5 dB. Comparison of our single-jet spectra with those from NASA large-scale jet facilities, and with the Tam et al.<sup>29</sup> similarity spectra, shows excellent agreement both in the spectral shape and in the value of overall sound pressure level (OASPL).<sup>30</sup>

The coordinates of the nozzle arrangement used are shown in Fig. 9. The primary and secondary nozzles were both convergent. The primary (core) nozzle terminated in a diameter  $D_p = 14.8$  mm and lip thickness of 0.7 mm. A 10-mm-diam axisymmetric plug reduced the effective (area-based) diameter of the primary nozzle to  $D_{p,\text{eff}} = 10.0$  mm. The secondary (bypass) nozzle terminated in a diameter of 25.4 mm. The exit planes of the two nozzles coincided. The contraction ratio was 4:1 for the core nozzle and 15:1 for the bypass nozzle. The Reynolds number of the primary jet was  $0.5 \times 10^6$ . Flexure of the pipe supporting the inner nozzle enabled coaxial and eccentric arrangements.

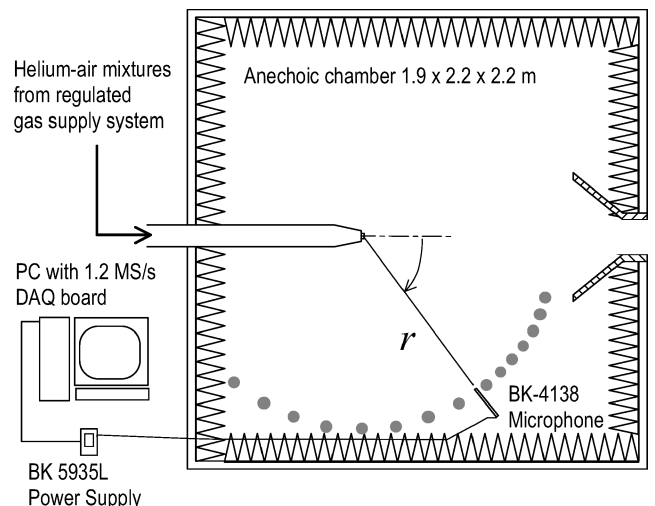


**Fig. 8** Jet aeroacoustics facility.

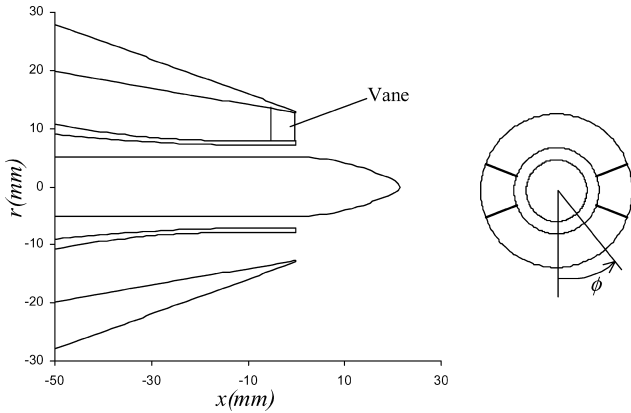


**Fig. 9** Coordinates of nozzle with axial and azimuthal placements of vanes.

Figure 9 also shows the vane placement for the experiment described in this paper. This was one of many arrangements tried in our laboratory in an effort to identify optimal arrangements that reduce both downward and sideline noise. The vanes were flat-plate, rectangular airfoils cut from 0.5-mm-thick sheet metal and glued to the outer surface of the inner nozzle. Two pairs of vanes were used. The trailing edges of the first pair were at azimuth angles  $\phi = \pm 70$  deg and those of the second pair were at  $\phi = \pm 110$  deg. Each vane was  $4 \times 4$  mm in size and spanned almost the entire width of the annulus of the bypass duct. The trailing edges of all of the vanes coincided with the nozzle exit plane. Based on one-dimensional approximation of the internal flow, the Mach numbers at the leading and trailing edge of each vane were calculated to be 0.60 and 0.95, respectively. Thus, each vane experienced an average freestream Mach number of 0.76. All of the vanes were placed at an angle of attack of approximately 11 deg to turn the flow in the downward direction.

Based on the aforementioned dimensions of the vanes and bypass duct, the vane impact factor [Eq. (12)] was  $\beta = 0.05$ . For  $\alpha = 11$  deg and with the assumption that  $a_{2D} = 0.08 \text{ deg}^{-1}$ , Eq. (14) gives  $C_L = 0.71$  and Eq. (15) gives  $\epsilon = 4.3$  deg. The lift coefficient is comfortably below 1.0, which precludes significant flow separation over the vanes. The total lift force of the vanes is 7% of the total thrust. When Eq. (18) is used with  $C_{D_p} = 0.015$ ,  $K = 0.4$ ,  $U_\infty = 80$  m/s, and the conditions of Table 1, the thrust loss with vanes at  $\alpha = 11$  deg is estimated at 0.5%. With the vanes deactivated ( $\alpha = 0$  deg), the thrust loss is 0.15%.

Based on the calculated pressure distribution in the clean duct, each vane was subjected to a normalized pressure gradient

$$\frac{c}{p} \frac{dp}{dx} = -0.3$$

with the reference pressure  $p$  evaluated at the leading edge of the vane. This is a very strong favorable gradient that is likely to improve airfoil performance, especially at high angles of attack.

## IV. Acoustic Results

### A. Noise Spectra and OASPL

This section compares the spectra for jets issuing from the three nozzles used in this study: clean coaxial (B60-COAX), eccentric (B60-ECC), and coaxial with vanes in the bypass stream (B60-VANES). For the asymmetric cases, an extra suffix denotes the azimuth angle of the microphone measurement. The frequency has been scaled up to match an exhaust with static thrust of 90 kN. The scale factor (the square root of the ratio of the engine thrust to the calculated laboratory jet thrust) was 41. First we examine the acoustic field in the downward direction of peak emission ( $\theta = 30$  deg) and on the plane  $\phi = 0$  deg. As seen in Fig. 10, the deflection of the bypass stream creates a substantial and across-the-board reduction of the spectrum. At full-scale frequencies in the range of 200–500 Hz

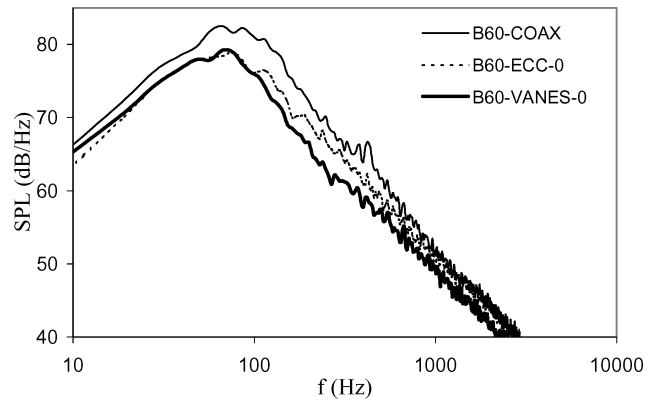


**Fig. 10** Spectra in the downward direction of peak sound emission ( $\theta = 30$  deg) and on the vertical plane ( $\phi = 0$  deg).

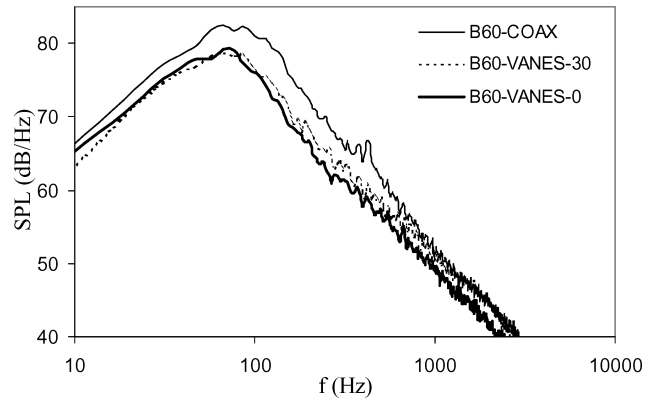


**Fig. 11** Comparison between the spectra of the coaxial jet with vanes in the downward direction of peak sound emission ( $\theta = 30$  deg) and at azimuth angles  $\phi = 0$  and 30 deg.

(which weigh heavily in perceived noise metrics), B60-VANES offers a reduction of about 6 dB, whereas B60-ECC reduces sound by only about 3 dB. The reduction becomes progressively smaller as the frequency increases. The same trends have been observed in higher-speed jets with  $B = 3$  using eccentric nozzles and nozzles with vanes.<sup>12</sup> A preliminary explanation is as follows. The sources of high-frequency, large-scale noise reside near the nozzle exit.<sup>19</sup> For moderate-to-high bypass ratios, the secondary core of the clean coaxial jet is long enough to cover this region and reduce  $M_c$  of the high-frequency instability waves. Thus, we should not expect a substantial reduction in high-frequency noise by offsetting or tilting the bypass stream. However, for the low-to-medium frequency noise sources, which reside farther downstream, the secondary core of the clean coaxial jet is too short to reduce  $M_c$  (Fig. 5). This noise source region can only be covered by offsetting or tilting the bypass stream, which explains the reduction at the low-to-midfrequencies seen in Fig. 10. Note that, for very low-bypass ratios (on the order of 1 or less), offsetting the nozzles causes large reductions in high-frequency noise.<sup>10</sup> There, the secondary core of the coaxial jet is just too short to cover adequately even the high-frequency noise sources. Also, low-bypass configurations have inherently high-speed cores. There is some evidence that, as the jet speed increases, the location of high-frequency noise sources moves downstream and can reach the end of the potential core.<sup>19,31</sup>

Figure 11 shows a comparison of the peak-emission spectra of B60-COAX and B60-VANES at azimuth angles  $\phi = 0$  and 30 deg. The noise reduction at  $\phi = 30$  deg is only 1–2 dB less than the downward noise reduction, which indicates that this arrangement has good sideline characteristics. Figure 12 plots the downward-emitted spectra at  $\theta = 90$  deg. This direction is dominated by noise from fine-scale turbulence, which of course is not the target of the method under consideration. The spectra of B60-COAX

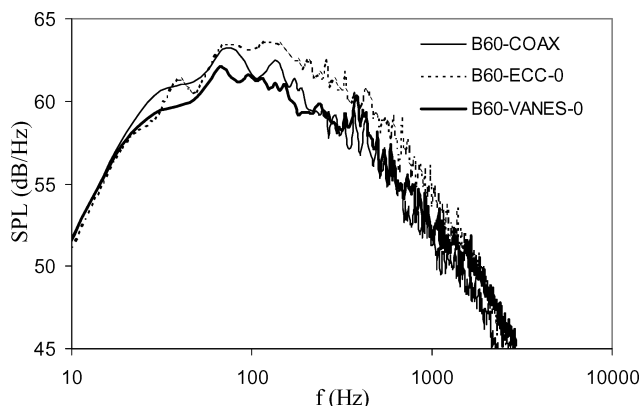


Fig. 12 Spectra at  $\theta = 90$  deg and  $\phi = 0$  deg.

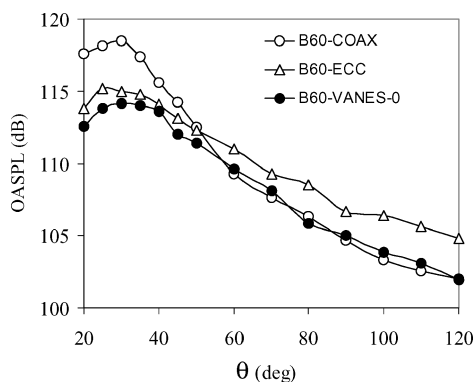


Fig. 13 Directivity of OASPL.

and B60-VANES-0 practically overlap, indicating no adverse effect of the vanes on laterally emitted noise. The spectrum of B60-ECC, on the other hand, displays a noticeable increase of 2–3 dB. The origin of this noise source is not yet known, but it must be associated with the complex flowpath formed by offsetting the nozzles. In the upper hemisphere, the spectra of B60-VANES practically match those of B60-COAX. Therefore, deflection of the bypass stream does not create additional noise in the upward direction. The upward-emitted spectra of B60-ECC were not measured here, but previous experience with eccentric configurations indicates that noise in the upward direction equals that of the primary (core) jet. Eccentric jets are, thus, noisier in the upward direction.

Figure 13 plots the directivity of OASPL on the plane  $\phi = 0$  deg for all of the cases investigated. The eccentric and deflected jets produce a significant decrease in the peak value of OASPL. It drops by 3.5 dB in B60-ECC and by 4.5 dB in B60-VANES. For B60-VANES, reduction in OASPL occurs for angles up to  $\theta = 60$  deg, after which the OASPL levels match those of B60-COAX. For the eccentric case, a crossover occurs at  $\theta = 50$  deg, and sound increases for the higher angles. Even though the eccentric nozzle reduces the peak OASPL appreciably, the noise increase at large angles penalizes its perceived noise performance, as will be shown in the next section. Clearly, the deflection approach is superior in that it suppresses better the peak levels of OASPL and prevents noise increase in the lateral direction.

## B. Perceived Noise Level

In Federal Air Regulations (FAR), aircraft noise is quantified in terms of the effective perceived noise level (EPNL), a metric that incorporates the human annoyance to sound.<sup>32</sup> Calculation of EPNL is an important exercise because it includes crucial effects not captured by laboratory spectra and OASPL plots: distance from the source, atmospheric absorption, and human perception. The absolute levels of EPNL will not be accurate because the effect of forward flight on jet acoustics was not present in the experiments. However, the estimated reduction in perceived noise provides valuable guidance.

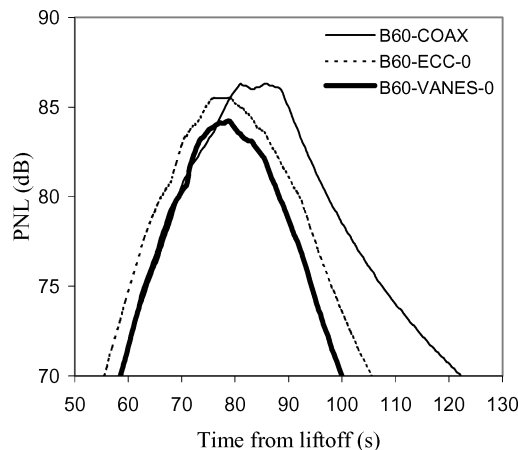


Fig. 14 History of perceived noise level recorded by takeoff monitor.

Note that other sources of noise, such as fan/compressor and airframe, are obviously not included in this assessment. The emphasis here is on noise recorded from the takeoff monitor for a full-power takeoff. Future studies will address takeoff with power cutback and noise recorded by the sideline and approach monitors.

We consider a twin-engine aircraft with each engine producing 90 kN of thrust. The flight path comprises a takeoff roll of 1500 m followed by a straight climb at climb angle of 12 deg, geometric angle of attack of 8 deg, and flight Mach number  $M_\infty = 0.32$ . The detailed steps involved in estimating the time history of perceived noise level [PNL( $t$ )] are covered in Ref. 11. The maximum level of PNL (PNLM) is calculated from PNL( $t$ ). The duration of PNL exceeding PNLM-10 dB is calculated, and the corresponding duration correction is computed according to FAR 36 (Ref. 32). The EPNL equals PNLM plus the duration correction. This estimate of EPNL does not include the tone correction, a penalty for excessively protrusive tones in the one-third-octave spectrum (which are absent from our spectra anyway).

Figure 14 shows a comparison of the PNL time history of the coaxial, eccentric, and coaxial with vanes jets. Relative to the clean coaxial exhaust, the coaxial exhaust with vanes reduces PNLM by 2.1 dB and the PNLM-10 duration by 18%. The corresponding reductions for the eccentric exhaust are 0.7 dB and 6%. In both the eccentric and vane configurations, the reduction in PNLM is associated with the reduction in peak noise seen in the spectra of Fig. 11 and in the OASPL plot of Fig. 14. Of particular importance is the spectral reduction in the frequency range 200–500 Hz. For times past the occurrence of PNLM, noise suppression becomes very pronounced, especially for B60-VANES. The corresponding emission angles are close to the jet axis, and the acoustic field is dominated by noise generated from large-scale structures. Before the occurrence of PNLM, the emission angles are large so that noise from fine-scale turbulence dominates. For those times, the PNL curves of B60-COAX and B60-VANES coincide. However, the curve of B60-ECC shows an increase of a few decibels, consistent with the spectral rise seen in Fig. 12 and the OASPL rise at large angles seen in Fig. 13. Thus, the eccentric configuration suffers a penalty in perceived noise because of the increase in laterally emitted noise. The EPNL results are as follows: 89.3 dB for B60-COAX, 88.3 dB for B60-ECC, and 86.5 dB for B60-VANES. In other words, the deflection of the bypass stream resulted in suppression of EPNL by 2.8 dB, whereas the eccentric nozzle produced a reduction of only 1.0 dB.

## V. Conclusions

The technique presented here reshapes the mean flowfield of the jet to create a long secondary core that reduces the convective Mach number throughout the noise source region of the primary jet. Downward tilting of the secondary plume relative to the primary plume is an effective means for such reshaping. The noise spectra in the downward direction of peak emission undergo a marked reduction across

all frequencies. Several additional factors must be investigated and modeled, however, before arriving at a thorough understanding of the noise reduction mechanism. They include the amplitude modulation  $A(x)$  for a disturbance at fixed frequency [Eq. (3)], the effect of the secondary core thickness and velocity nonuniformity on sound attenuation, and the relation between the azimuthal thickness of the secondary core and corresponding azimuthal distribution of noise reduction.

The experience in our laboratory indicates that the overall performance of this method depends on the details of the devices used for reshaping the mean flow. In the case of tilting of the bypass stream, noise reduction is sensitive to the shape and size of the deflector vanes, their azimuthal and axial locations, and their angle of attack. The configuration presented here (Fig. 9) is one of the better arrangements tested so far but probably not the ultimate design. There is a very large parameter space to explore, including variation of the nozzle geometry, and so the potential exists for even larger noise reductions than those presented here. A computational effort, currently in progress, will provide accurate predictions of lift and drag of the vanes, and, therefore, will guide the experimental effort toward designs that are optimal for noise reduction and aerodynamic efficiency.

An important missing piece of the puzzle is the effect of forward flight, which cannot be simulated in the present experiment. Forward flight will definitely reduce the secondary convective Mach number  $M_{cs}$ . The results of Fig. 5 suggest that, by offsetting or tilting the bypass stream, large-scale noise is governed by  $M_{cs}$  rather than  $M_{cp}$ . A reduction in  $M_{cs}$  will lead to a much quieter secondary core and will, therefore, enhance the effect of reducing  $M_{cp}$ . At the same time, forward flight is expected to stretch the secondary core, thus, providing better coverage of the primary noise source region. Thus, the expectation is that forward flight will amplify the benefit of this technique. The future plan is to test these conjectures by analytical models, computations, and large-scale tests.

### Acknowledgments

This research has been supported by NASA John H. Glenn Research Center at Lewis Field (Grant NAG-3-2345 monitored by Khairul B. Zaman). Kimberley Nishi is thanked for conducting the jet experiments. The method and system of noise suppression via deflection of the bypass and/or core streams is proprietary to the University of California, U.S. Patent Pending.

### References

- <sup>1</sup>Tam, C. K. W., and Chen, P., "Turbulent Mixing Noise from Supersonic Jets," *AIAA Journal*, Vol. 32, No. 9, 1994, pp. 1774–1780.
- <sup>2</sup>Tam, C. K. W., "Jet Noise: Since 1952," *Theoretical and Computational Fluid Dynamics*, Vol. 10, Jan. 1998, pp. 393–405.
- <sup>3</sup>Saiyed, N. H., Mikkelsen, K. L., and Bridges, J. E., "Acoustics and Thrust of Separate-Flow High-Bypass-Ratio Engines," *AIAA Journal*, Vol. 41, No. 3, 2003, pp. 372–378.
- <sup>4</sup>McLaughlin, D. K., Morrison, G. D., and Troutt, T. R., "Experiments on the Instability Waves in a Supersonic Jet and Their Acoustic Radiation," *Journal of Fluid Mechanics*, Vol. 69, No. 11, 1975, pp. 73–95.
- <sup>5</sup>Troutt, T. R., and McLaughlin, D. K., "Experiments on the Flow and Acoustic Properties of a Moderate Reynolds Number Supersonic Jet," *Journal of Fluid Mechanics*, Vol. 116, March 1982, pp. 123–156.
- <sup>6</sup>Tam, C. K. W., and Burton, D. E., "Sound Generated by Instability Waves of Supersonic Flows, Part 2. Axisymmetric Jets," *Journal of Fluid Mechanics*, Vol. 138, 1984, pp. 249–271.
- <sup>7</sup>Seiner, J. M., Bhat, T. R. S., and Ponton, M. K., "Mach Wave Emission from a High-Temperature Supersonic Jet," *AIAA Journal*, Vol. 32, No. 12, 1994, pp. 2345–2350.
- <sup>8</sup>Mitchell, B. E., Lele, S. K., and Moin, P., "Direct Computation of Mach

Wave Radiation in an Axisymmetric Supersonic Jet," *AIAA Journal*, Vol. 35, No. 10, 1997, pp. 1574–1580.

<sup>9</sup>Mankbadi, R. R., Hixon, R., Shih, S.-H., and Povinelli, L. A., "Use of Linearized Euler Equations for Supersonic Jet Noise Prediction," *AIAA Journal*, Vol. 36, No. 2, 1998, pp. 140–147.

<sup>10</sup>Papamoschou, D., and Debiase, M., "Directional Suppression of Noise from a High-Speed Jet," *AIAA Journal*, Vol. 39, No. 3, 2001, pp. 380–387.

<sup>11</sup>Papamoschou, D., and Debiase, M., "Conceptual Development of Quiet Turbofan Engines for Supersonic Aircraft," *Journal of Propulsion and Power*, Vol. 18, No. 2, 2003, pp. 161–169.

<sup>12</sup>Papamoschou, D., "Engine Cycle and Exhaust Configuration for Quiet Supersonic Propulsion," *Journal of Propulsion and Power*, Vol. 20, No. 2, 2004, pp. 255–262; also AIAA Paper 2002-3917, 2002.

<sup>13</sup>Crighton, D. G., and Huerre, P., "Shear-Layer Pressure Fluctuations and Superdirective Acoustic Sources," *Journal of Fluid Mechanics*, Vol. 220, 1990, pp. 355–368.

<sup>14</sup>Avital, E. J., Sandham, N. D., and Luo, K. H., "Mach Wave Radiation in Mixing Layers. Part I: Analysis of the Sound Field," *Theoretical and Computational Fluid Dynamics*, Vol. 12, Sept. 1998, pp. 73–90.

<sup>15</sup>Freund, J. B., "Noise Sources in a Low-Reynolds-Number Turbulent Jet at Mach 0.9," *Journal of Fluid Mechanics*, Vol. 438, 2001, pp. 277–305.

<sup>16</sup>Panda, J., and Zaman, K. B. M. Q., "Density Fluctuation in Asymmetric Nozzle Plumes and Correlation with Far Field Noise," AIAA Paper 2001-0378, 2001.

<sup>17</sup>Panda J., and Seasholtz, R. G., "Experimental Investigation of Density Fluctuations in High-Speed Jets and Correlation with Generated Noise," *Journal of Fluid Mechanics*, Vol. 450, Jan. 2002, pp. 97–130.

<sup>18</sup>Hileman, J., and Samimy, M., "Turbulence Structures and the Acoustic Far Field of a Mach 1.3 Jet," *AIAA Journal*, Vol. 39, No. 9, 2001, pp. 1716–27.

<sup>19</sup>Narayanan, S., Barber, T. J., and Polak, D. R., "High Subsonic Jet Experiments: Turbulence and Noise Generation Studies," *AIAA Journal*, Vol. 40, No. 3, 2002, pp. 430–437.

<sup>20</sup>Murakami, E., and Papamoschou, D., "Eddy Convection in Supersonic Coaxial Jets," *AIAA Journal*, Vol. 38, No. 4, 2000, pp. 628–635.

<sup>21</sup>Murakami, E., and Papamoschou, D., "Mean Flow Development of Dual-Stream Compressible Jets," *AIAA Journal*, Vol. 40, No. 6, 2002, pp. 1131–1138.

<sup>22</sup>Dahl, M. D., and Morris, P. J., "Noise from Supersonic Coaxial Jets, Part I: Mean Flow Predictions," *Journal of Sound and Vibration*, Vol. 200, No. 5, 1997, pp. 643–663.

<sup>23</sup>Papamoschou, D., "A New Method for Jet Noise Reduction in Turbofan Engines," AIAA Paper 2003-1059, 2003.

<sup>24</sup>Shevell, R. S., *Fundamentals of Flight*, 2nd ed., Prentice-Hall, Upper Saddle River, NJ, 1989, pp. 146, 147, 186.

<sup>25</sup>Kim, S., Alonso, J. J., and Jameson, A., "Design Optimization of High-Lift Configurations Using a Viscous Continuous Adjoint Method," AIAA Paper 2002-0844, Jan. 2002.

<sup>26</sup>Ladson, C. L., "Two-Dimensional Airfoil Characteristics of Four NACA 6A-Series Airfoils at Transonic Mach Numbers up to 1.25," NACA RM L57F05, Aug. 1957.

<sup>27</sup>Kinzie, K. W., and McLaughlin, D. K., "Measurements of Supersonic Helium/Air Mixture Jets," *AIAA Journal*, Vol. 37, No. 11, 1999, pp. 1363–1369.

<sup>28</sup>Papamoschou, D., and Debiase, M., "Noise Measurements in Supersonic Jets Treated with the Mach Wave Elimination Method," *AIAA Journal*, Vol. 37, No. 2, 1999, pp. 154–160.

<sup>29</sup>Tam, C. K. W., Golebiowski, M., and Seiner, J., "On the Two Components of Turbulent Mixing Noise from Supersonic Jets," AIAA Paper 96-1716, 1996.

<sup>30</sup>*Proceedings of the Jet Noise Workshop*, NASA CP-2001-211152, Nov. 2001.

<sup>31</sup>Mohseni, K., Colonius, T., and Freund, J. B., "An Evaluation of Linear Instability Waves as Sources of Sound in a Supersonic Turbulent Jet," *Physics of Fluids*, Vol. 14, No. 10, 2002, pp. 3593–3600.

<sup>32</sup>"Noise Standards: Aircraft Type and Airworthiness Certification," Federal Aviation Administration, Federal Aviation Regulations, Pt. 36, Washington, DC, Jan. 2001.

W. Devenport  
Associate Editor